

Stephan Baer  
Klaus Ensslin

# Transport Spectroscopy of Confined Fractional Quantum Hall Systems



Springer

# **Springer Series in Solid-State Sciences**

Volume 183

## **Series editors**

Bernhard Keimer, Stuttgart, Germany

Roberto Merlin, Ann Arbor, MI, USA

Hans-Joachim Queisser, Stuttgart, Germany

Klaus von Klitzing, Stuttgart, Germany

The Springer Series in Solid-State Sciences consists of fundamental scientific books prepared by leading researchers in the field. They strive to communicate, in a systematic and comprehensive way, the basic principles as well as new developments in theoretical and experimental solid-state physics.

More information about this series at <http://www.springer.com/series/682>

Stephan Baer · Klaus Ensslin

# Transport Spectroscopy of Confined Fractional Quantum Hall Systems



Springer

Stephan Baer  
Solid State Physics Laboratory  
ETH Zürich  
Zürich  
Switzerland

Klaus Ensslin  
Solid State Physics Laboratory  
ETH Zürich  
Zürich  
Switzerland

ISSN 0171-1873                    ISSN 2197-4179 (electronic)  
Springer Series in Solid-State Sciences  
ISBN 978-3-319-21050-6        ISBN 978-3-319-21051-3 (eBook)  
DOI 10.1007/978-3-319-21051-3

Library of Congress Control Number: 2015944176

Springer Cham Heidelberg New York Dordrecht London  
© Springer International Publishing Switzerland 2015

This work is subject to copyright. All rights are reserved by the Publisher, whether the whole or part of the material is concerned, specifically the rights of translation, reprinting, reuse of illustrations, recitation, broadcasting, reproduction on microfilms or in any other physical way, and transmission or information storage and retrieval, electronic adaptation, computer software, or by similar or dissimilar methodology now known or hereafter developed.

The use of general descriptive names, registered names, trademarks, service marks, etc. in this publication does not imply, even in the absence of a specific statement, that such names are exempt from the relevant protective laws and regulations and therefore free for general use.

The publisher, the authors and the editors are safe to assume that the advice and information in this book are believed to be true and accurate at the date of publication. Neither the publisher nor the authors or the editors give a warranty, express or implied, with respect to the material contained herein or for any errors or omissions that may have been made.

Printed on acid-free paper

Springer International Publishing AG Switzerland is part of Springer Science+Business Media  
([www.springer.com](http://www.springer.com))

# Preface

At very low temperatures and at certain filling factors  $\nu$ , the ground state of a high mobility electron gas exposed to a strong magnetic field becomes incompressible, forming an integer quantum Hall (IQH) or fractional quantum Hall (FQH) state. The  $\nu = 5/2$  state is one of the most exceptional of these states, as it is believed to exhibit non-Abelian quasiparticle excitations. This property makes it not only interesting from a fundamental physics point of view, but also for possible applications in topological quantum computing.

In this book, we investigate the properties of the IQH and FQH states, using transport measurements in the bulk, in quantum point contacts (QPCs) and through quantum dots (QDs) or interferometers implemented in high mobility GaAs samples. One important goal of the work presented in this book has been to study the properties of the  $\nu = 5/2$  state by investigating its tunneling and confinement properties and to make progress towards the realization of an experiment that allows to probe the statistics of the quasiparticle excitations at  $\nu = 5/2$ .

This book gives an insight into the work on the  $\nu = 5/2$  state that has been conducted at ETH Zürich in a collaboration of the groups of Werner Wegscheider and Klaus Ensslin, since 2010. The book is based on a dissertation written by Stephan Baer in the group of Klaus Ensslin [1].

This book provides an overview of recent developments in experiments probing the fractional quantum Hall (FQH) states of the second Landau level, especially the  $\nu = 5/2$  state. It summarizes the state-of-the-art understanding of these FQH states. It furthermore describes how the properties of the FQH states can be probed experimentally, by investigating tunneling and confinement properties. The progress towards the realization of an experiment, allowing to probe the potentially non-Abelian statistics of the quasiparticle excitations at  $\nu = 5/2$  is discussed. The book is intended as a reference for graduate students and postdocs starting in the field. The experimental part of this book gives practical advice for solving the experimental challenges which are faced by researchers studying highly fragile FQH states.

We thank the following colleagues for their contribution to this work or for discussions: Clemens Rössler, Thomas Ihn, Szymon Hennel, Werner Wegscheider,

Christian Reichl, Anastasia Varlet, Tobias Krähenmann, Ernst de Wiljes,  
Per-Lennart Ardelt, Thomas Hasler, Hiske Overweg, Sebastian Butz, Dominic  
Blosser, Bernd Rosenow, Rudolf Morf, Lars Tiemann and many others.

Zürich  
July 2015

Stephan Baer  
Klaus Ensslin

## Reference

1. S. Baer, Transport spectroscopy of confined fractional quantum Hall systems, Ph.D. thesis, ETH Zürich, Zürich, 2014. <http://dx.doi.org/10.3929/ethz-a-010252603>

# Contents

<b>1</b>	<b>Introduction . . . . .</b>	<b>1</b>
	References. . . . .	5
 <b>Part I Fundamentals of Quantum Hall Physics and Relevant Experiments</b>		
<b>2</b>	<b>Two-Dimensional Electron Gases . . . . .</b>	<b>9</b>
2.1	Introduction . . . . .	9
2.2	Basic Properties of Two-Dimensional Electron Gases . . . . .	10
2.3	Low Field Magnetoresistance of Two-Dimensional Electron Gases . . . . .	14
2.4	Growth Schemes for High Electron Mobilities . . . . .	16
2.5	Impact of Disorder on the Gap of the $\nu = 5/2$ State . . . . .	18
	References. . . . .	20
<b>3</b>	<b>The Quantum Hall Effect . . . . .</b>	<b>21</b>
3.1	Introduction . . . . .	21
3.2	Energy Spectrum in a Magnetic Field . . . . .	21
3.3	Shubnikov-De Haas Effect . . . . .	24
3.4	Integer Quantum Hall Effect. . . . .	25
3.4.1	Landauer-Büttiker Formalism . . . . .	26
3.4.2	Many-Body Wavefunction of the Lowest Landau Level . . . . .	29
3.5	Fractional Quantum Hall Effect . . . . .	29
3.5.1	Laughlin's Wavefunction . . . . .	30
3.5.2	Composite Fermion Theory . . . . .	31
3.6	Fractional Quantum Hall Effect in the Second Landau Level . . . . .	34
3.6.1	Candidate States for $\nu = 5/2$ . . . . .	35
3.6.2	Candidate States for $\nu = 7/3$ and $\nu = 8/3$ . . . . .	39

3.6.3	Candidate States for $\nu = 12/5$ . . . . .	41
3.7	Conclusion . . . . .	43
	References . . . . .	43
<b>4</b>	<b>Physics at the Edge . . . . .</b>	<b>47</b>
4.1	Introduction . . . . .	47
4.2	Spatial Edge State Picture . . . . .	47
4.2.1	Self-consistency at the Edge . . . . .	48
4.2.2	FQH Edge States . . . . .	50
4.3	Energetic Edge State Picture. . . . .	55
4.3.1	Hydrodynamic Theory . . . . .	55
4.3.2	Hierarchical States and Bulk-Edge Correspondence . . . . .	58
4.3.3	Tunneling in a QPC . . . . .	58
	References . . . . .	61
<b>5</b>	<b>Non-Abelian Statistics and Its Signatures in Interference Experiments . . . . .</b>	<b>63</b>
5.1	From Fermions to Anyons . . . . .	63
5.2	Non-Abelian Anyons in the Moore-Read Pfaffian State . . . . .	64
5.3	Interferometry with Non-Abelian Anyons. . . . .	66
5.4	Aharonov-Bohm Versus Coulomb-Dominated Physics . . . . .	67
	References . . . . .	70
<b>6</b>	<b>Overview of Experiments Probing the Properties of the <math>\nu = 5/2</math> State . . . . .</b>	<b>73</b>
6.1	Introduction . . . . .	73
6.2	Numerical Studies . . . . .	74
6.3	Detecting the Quasiparticle Charge . . . . .	75
6.3.1	Shot Noise Measurements . . . . .	75
6.3.2	Local Compressibility Measurements. . . . .	76
6.4	Bulk Experiments: Probing the Spin Polarization . . . . .	76
6.4.1	Transport: Density Dependence of the Gap . . . . .	77
6.4.2	Transport: In-Plane Magnetic Fields . . . . .	79
6.4.3	Optics . . . . .	80
6.4.4	Nuclear Magnetic Resonance Techniques. . . . .	81
6.4.5	Conclusion . . . . .	82
6.5	Probing the Edge Properties . . . . .	82
6.5.1	Quasiparticle Tunneling . . . . .	82
6.5.2	Neutral Mode Experiments. . . . .	84
6.6	Interference Experiments at $\nu = 5/2$ . . . . .	86
6.7	Summary . . . . .	90
	References . . . . .	91

**Part II Setup and Sample Optimization**

<b>7 Measurement Setup Optimization for Low Electron Temperatures</b> . . . . .	97
7.1 Introduction . . . . .	97
7.2 Dilution Refrigerator Setup . . . . .	98
7.2.1 Vibration Minimization and Insulation . . . . .	101
7.2.2 Electronic Noise . . . . .	106
7.3 Cryostat Cabling and Cold Filtering . . . . .	108
7.3.1 General Remarks . . . . .	108
7.3.2 Thermocoax Cables . . . . .	111
7.3.3 $\pi$ -Filters . . . . .	111
7.3.4 Quartz Heat Sinks . . . . .	112
7.3.5 RC Low-Pass Filters . . . . .	113
7.3.6 Silver Cold-Finger . . . . .	113
7.3.7 Filter Attenuation . . . . .	115
7.4 Estimation of the Electronic Temperature . . . . .	117
7.5 Outlook . . . . .	120
7.6 Conclusion . . . . .	121
References . . . . .	121
<b>8 Optimization of Samples and Sample Fabrication</b> . . . . .	123
8.1 Introduction . . . . .	123
8.2 Non-invasive Processing . . . . .	123
8.3 Mesa and Contact Geometry . . . . .	125
8.4 Ohmic Contacts and Contact Resistance . . . . .	127
8.5 Conclusion . . . . .	129
References . . . . .	129

**Part III Quantum Point Contact Experiments**

<b>9 Quantum Point Contacts</b> . . . . .	133
9.1 Introduction . . . . .	133
9.2 Conductance of Ideal and Non-ideal QPCs . . . . .	135
9.2.1 Transmission of an Ideal Quantum Wire . . . . .	135
9.2.2 Non-ideal QPC . . . . .	137
9.2.3 Saddle-Point Potential . . . . .	138
9.2.4 Magneto-Electric Depopulation . . . . .	139
9.3 QPC Simulations . . . . .	139
9.4 Transport Properties of Clean QPCs . . . . .	142
9.4.1 Lateral Shifting of the QPC Channel . . . . .	142
9.4.2 Finite Bias Transmission . . . . .	143
9.4.3 Tuning the QPC Confinement Potential . . . . .	147

9.4.4	Spin-Resolved Transport . . . . .	151
9.4.5	Bias Dependence in the Quantum Hall Regime. . . . .	153
9.5	Conclusion. . . . .	155
	References. . . . .	156
<b>10</b>	<b>Integer and Fractional Quantum Hall States in QPCs</b> . . . . .	159
10.1	Introduction . . . . .	159
10.2	Experimental Details . . . . .	161
10.3	Results and Discussion . . . . .	162
10.3.1	Quantum Hall Phase Diagram of a QPC . . . . .	162
10.3.2	Influence of QPC Geometry on Incompressible Separating Region and Density Distribution . . . . .	165
10.3.3	Characterization of QPC Resonances and Microscopic Model . . . . .	167
10.3.4	Spatial Dependence of QPC Resonances . . . . .	174
10.3.5	Fragile Fractional Quantum Hall States in QPCs . . . . .	177
10.3.6	Energy Gap of the $\nu_{\text{QPC}} = 1/3$ State . . . . .	180
10.4	Conclusion. . . . .	183
	References. . . . .	184
<b>11</b>	<b>Quasiparticle Tunneling in the Second Landau Level</b> . . . . .	187
11.1	Introduction . . . . .	187
11.2	Experimental Details . . . . .	189
11.3	Measurement Results. . . . .	189
11.3.1	Tunneling Conductance at $\nu = 5/2$ . . . . .	191
11.3.2	Tunneling Conductance at $\nu = 8/3$ . . . . .	195
11.3.3	Effect of Varying the Coupling via the Magnetic Field . . . . .	198
11.3.4	Effect of Varying the Coupling via the QPC Transmission. . . . .	200
11.3.5	Breakdown of the Weak Tunneling Regime . . . . .	201
11.4	Interpretation and Discussion . . . . .	202
11.4.1	$\nu = 8/3$ . . . . .	202
11.4.2	$\nu = 5/2$ . . . . .	203
11.4.3	$\nu = 7/3$ . . . . .	204
11.4.4	Experimental Limitations and Origin of Systematic Errors . . . . .	205
11.5	Conclusion . . . . .	206
	Appendix . . . . .	207
	FWHM of Tunneling Peaks . . . . .	207
	Fits for Proposed Parameter Pairs— $\nu = 5/2$ . . . . .	207
	Fits for Proposed Parameter Pairs— $\nu = 8/3$ . . . . .	208
	Additional Fits— $V_{\text{QPC}}$ Dependence . . . . .	209
	References. . . . .	215

**Part IV Quantum Dot and Interferometer Experiments**

<b>12 Quantum Dots and Charge Detection Techniques</b> . . . . .	221
12.1 Introduction . . . . .	221
12.2 Basics of Quantum Dots . . . . .	222
12.2.1 Energy Scales. . . . .	222
12.2.2 Coulomb Blockade . . . . .	223
12.2.3 Principle of Charge Detection. . . . .	225
12.3 Improving the Charge Detection Sensitivity . . . . .	226
12.4 Conclusion. . . . .	230
References. . . . .	231
<b>13 Quantum Dots in the Quantum Hall Regime</b> . . . . .	233
13.1 Introduction . . . . .	233
13.2 Experimental Details . . . . .	234
13.3 Results and Discussion . . . . .	235
13.3.1 Zero Magnetic Field Transport . . . . .	235
13.3.2 Non-cyclic Depopulation of Edge Channels . . . . .	235
13.3.3 Transport in the Fabry-Pérot Regime. . . . .	243
13.4 Conclusion. . . . .	245
References. . . . .	245
<b>14 Preliminary Results of Interference Experiments in the Second Landau Level</b> . . . . .	247
14.1 Introduction . . . . .	247
14.2 Design Considerations . . . . .	248
14.3 Transport Measurements . . . . .	250
14.3.1 Sample Stability Issues . . . . .	251
14.3.2 Optimizing the Transmission by Sample Illumination . . . . .	253
14.4 Conclusion and Outlook . . . . .	261
References. . . . .	261

**Part V Bulk Transport Experiments**

<b>15 Non-equilibrium Transport in Density Modulated Phases of the Second Landau Level</b> . . . . .	265
15.1 Introduction . . . . .	265
15.2 Experimental Details . . . . .	266
15.3 Results and Discussion . . . . .	267
15.3.1 Phase Diagram of Reentrant Integer Quantum Hall Phases . . . . .	269

15.3.2	Transition from RIQH Phase to Isotropic Compressible Phase . . . . .	271
15.3.3	Discussion of the Bias Dependence. . . . .	274
15.3.4	Reentrant Integer Quantum Hall Phases in a QPC . . . . .	276
15.3.5	Orientation Dependence. . . . .	278
15.4	Conclusion. . . . .	279
Appendix	. . . . .	280
	Dependence on Magnetic Field Direction. . . . .	280
	Hysteresis of Current Sweeps . . . . .	280
	Negative Differential Resistance from DC Measurement . . . . .	280
	Bias Dependence of the Longitudinal Resistance. . . . .	281
	References. . . . .	283
 <b>Part VI Conclusion</b>		
<b>16</b>	<b>Conclusion</b> . . . . .	289
<b>Appendices</b>	. . . . .	293
<b>Index</b>	. . . . .	305

# Symbols and Abbreviations

## Physical Constants

$a_B$	Bohr radius
$-e < 0$	Electron charge
$\epsilon$	Dielectric permittivity
$\epsilon_0$	Vacuum dielectric constant
$h = 2\pi\hbar$	Planck's constant
$k_B$	Boltzmann constant
$\mu_B$	Bohr magneton
$R_K = h/e^2$	Von Klitzing constant

## Symbols

$L, W$	System size (length, width)
$B$	Magnetic field
$\vec{A}$	Vector potential
$E_C$	Constant interaction energy
$\alpha_G$	Gate lever arm
$\Delta_N$	Spin degenerate single particle level spacing
$E_F$	Fermi energy
$Q$	Charge
$I$	Current
$V$	Voltage
$G$	Conductance
$\rho$	Resistance
$v_F$	Fermi velocity
$k_F$	Fermi wavenumber
$\lambda_F$	Fermi wavelength
$l_B$	Magnetic length
$l_e$	Elastic mean free path

$\tau_{tr}$	Transport scattering time
$\tau_q$	Quantum life time
$m^*$	Effective electron mass in GaAs
$\mu$	Electron mobility
$n_s$	Electron sheet density
$\nu$	Filling factor
$\nu_{QPC}$	QPC filling factor
$\nu_{\text{bulk}}$	Bulk filling factor
$\omega_c$	Cyclotron frequency
$r_c$	Cyclotron radius
$\omega_y, \omega_x$	Confinement strength of a harmonic potential
$r_s$	Interaction parameter
$g^*$	Effective g-factor
$T$	Temperature

## Abbreviations

2DEG	Two-dimensional electron gas
AC	Alternating current
AFM	Atomic force microscope
CB	Coulomb blockade
CF	Composite Fermion
DC	Direct current
DOS	Density of states
ES	Excited state
FIRST	Frontiers in research, space and time (Cleanroom at ETH Zürich)
FQH(E)	Fractional quantum Hall (effect)
FWHM	Full width at half maximum
GS	Ground state
IQH(E)	Integer quantum Hall (effect)
LL	Landau level
MBE	Molecular beam epitaxy
QD	Quantum dot
QPC	Quantum point contact
RIQH(E)	Reentrant integer quantum Hall (effect)
SdH	Shubnikov de Haas

# Chapter 1

## Introduction

*This work contains many things which are new and interesting.  
Unfortunately, everything that is new is not interesting, and  
everything which is interesting, is not new.*

Lev Landau, not in reference to this book

### Motivation

Some of the most intriguing physical phenomena, like superconductivity, superfluidity or Bose-Einstein condensation, are many-body effects. Here the interaction of the particles that constitute the physical system can change the system's behavior dramatically. Many of these effects have been discovered unintentionally in experiments which were conducted for example at very low temperatures and in very pure or very regular systems. Under such conditions, interaction effects that otherwise do not play a role and which often were not anticipated, become relevant.

Two-dimensional electron gases (2DEGs) are the ideal system for the experimentalist studying many-body effects in solid state physics. These systems are exceptionally pure and can be cooled to temperatures below 10 mK with state-of-the-art experimental setups. The fractional quantum Hall (FQH) effect is a many-body effect that has been discovered under these conditions. Electrons in a two-dimensional system exposed to a strong magnetic field interact with each other via the Coulomb interaction. It turns out that under certain conditions electrons form a collective ground state, described by a many-body wavefunction proposed by Laughlin [1]. The interacting electrons in this state can be understood as new quasiparticles, so-called composite Fermions [2]. In this description, they are only weakly interacting and have different physical properties than the original electrons. For example, the charge of the quasiparticles no longer corresponds to the original electron charge, but is only a fraction of it. Another far-reaching consequence of the correlations in a two-dimensional system is that composite particles do not behave as Fermions or Bosons. While a particle exchange of Fermions or Bosons changes the phase of the wavefunction by 0 or  $\pi$ , it can be any value for the quasiparticles of the fractional quantum Hall effect, making them “anyons”.

With the chase for new physics, samples have been further improved, revealing new interesting phenomena. One of the most remarkable subsequent discoveries was the  $\nu=5/2$  state [3], which could no longer be understood in the framework developed for the ordinary FQH effect. A possible explanation for this groundstate suggests a BCS-like  $p$ -wave pairing of composite Fermions [4]. However, alternative less exciting explanations exist (see Sect. 3.6). The  $p$ -wave paired Moore-Read Pfaffian groundstate would possess another property, which has tremendously increased the interest in the  $\nu=5/2$  state: it is believed to exhibit non-Abelian anyonic excitations. In a very simplified picture, this can be understood in the following way [5]: given an ensemble of  $N$  quasiparticles, an exchange of two quasiparticles transforms the total wavefunction to a different final state. The system is said to be non-Abelian, if performing exactly the same exchange operations in a different sequence leads to a different final state. By exchanging quasiparticles in a particular sequence, this might allow to apply a desired unitary transformation to the wavefunction, which could for example be used for quantum computation. Here, the exact trajectories on which the quasiparticles are exchanged are irrelevant and the system is protected from decoherence. Such a system is said to be “topologically protected”.

Though numerical and first experimental results favor the non-Abelian candidates for  $\nu=5/2$ , the definite proof is still missing. Also the nature of most of the other FQH states in the second Landau level (LL), like the  $\nu=7/3$  and  $\nu=8/3$  FQH states is not fully clarified yet. Given the large theoretical effort that is invested to explore the potential properties of these states, answering the open questions is one of the most important experimental tasks in the quantum Hall research community.

However, even without non-Abelian statistics, the FQH states in the second LL contain interesting many-body physics and are worth studying. The physics in the second Landau level is not only influenced by FQH states, but also by electron crystal phases which compete with the FQH states. The properties of those states are still largely unexplored and require further experimental study.

## **Impact of this work and outlook**

An important goal of the experiments presented in this book was to investigate the properties of the FQH states in the second LL, especially the  $\nu=5/2$  state. Our work intends to advance towards the realization of an interference experiment that clarifies the nature of the  $\nu=5/2$  state and its potential suitability for quantum computing.

This book is the result of the first Ph.D. project conducted on the  $\nu=5/2$  state in the Ensslin group at ETH Zürich by Stephan Baer. Hence we describe the experimental tasks, necessary for starting this project. For example, it was necessary to improve a dry dilution refrigerator setup for low electronic temperatures and a new low temperature cabling, filtering setup and silver cold finger had to be designed and built. Furthermore the sample processing had to be carefully checked and optimized, in order to avoid a degradation of the quality of the 2DEGs. Due to a close collaboration with the Wegscheider group, we could identify and characterize wafers that exhibit a pronounced  $\nu=5/2$  state and which were suitable for the experiments conducted by us. By accomplishing these tasks we were finally able to observe the most fragile FQH states and could reach an electronic temperature of approximately

12–13 mK at a cryostat temperature of approximately 9–10 mK. Compared to the best electronic temperatures of around 50 mK that have been reached in the Ensslin group before, this is a large improvement. This preliminary work paves the way for future FQH experiments at very low temperatures in the Ensslin group. Starting from the prototype cabling and filtering employed by us, cold filtering techniques have been further improved. In the Ensslin group’s new cryostat with a base temperature of less than 3.5 mK, these developments might allow the study of even more fragile FQH states, like for example the  $\nu=12/5$  state.

Quantum point contacts (QPCs) allow a local manipulation of FQH states and are a basic building block for interferometers that try to investigate the  $\nu=5/2$  state. We have investigated the transport properties of QPCs fabricated on high-mobility electron gases. Finite-bias measurements have allowed us to investigate the confinement potential and its influence on the QPC transmission in magnetic fields. Here correlation effects show up in the transport. They arise from an interplay of the FQH states with localized states, which are described by single- or many-electron physics. In the FQH regime, disorder has a large influence on the transmission and we observe effects related to the localization of fractionally charged quasiparticles in the constriction. We have investigated the transmission properties of QPCs, which is necessary in order to be able to correctly interpret tunneling and interferometer experiments using QPCs, especially at  $\nu=5/2$ .

Gating high-mobility 2DEGs is experimentally challenging and requires optimizing the gating procedure to the doping scheme of the heterostructure. By doing this, we succeeded to define QPCs, with a perfect transmission of the  $\nu=5/2$  state. We have demonstrated that this state can survive fully gapped in a top-gate defined interferometer, with an energy gap exceeding 200 mK. This is a crucial prerequisite for interference experiments at this filling factor. To our knowledge, this has not been clearly demonstrated before.

Using the gating techniques, we were able to define a QPC in a weak backscattering regime, where quasiparticle tunneling in the FQH states at  $\nu=5/2$ ,  $7/3$  and  $8/3$  could be observed. Previous experiments were only conducted with a single sample and were not fully conclusive regarding the question whether the tunneling properties at  $\nu=5/2$  favor an Abelian (3,3,1)-state or the non-Abelian Anti-Pfaffian or SU(2)<sub>2</sub>-states. Hence, repeating those experiments with a different sample, fabricated with a different growth technique was desirable. Furthermore, a correct interpretation of the experiment in terms of the weak tunneling theory might depend sensitively on the experimental situation, like the backscattering strength and the local filling factor. We have addressed these open questions in detail and found that the Abelian (3,3,1)- and (1,1,3)-states describe our data best. Though this result is for example inconsistent with numerical findings, the quality of agreement of our data and theoretical predictions for the (3,3,1)- and (1,1,3)-states is astonishing. The nature of the  $\nu=8/3$  and  $7/3$  states is not fully clear and non-Abelian candidate states have also been proposed here. We present the first systematic investigation of these states in a tunneling experiment. We find that the  $\nu=8/3$  state is best described by a particle-hole conjugate Laughlin state. This finding is not only relevant for  $\nu=8/3$ , but is also an important crosscheck for the tunneling experiments that have investigated the  $\nu=5/2$  state. Our

quasiparticle tunneling experiments will be supplemented by further experiments at  $\nu=1/3$  and  $\nu=2/3$ , which are currently being performed in the Ensslin group. These studies might reveal whether additional interaction effects which have not been taken into account in the theory modify the quasiparticle tunneling signatures.

In addition to the QPC measurements, we have performed transport measurements of large quantum dots and interferometers in magnetic fields. We have optimized charge detection techniques, which allow a time-resolved single-electron charge detection on micron-sized quantum dots, which are suitable for interference experiments in the quantum Hall regime. In order to perform charge detection on such large QDs, the sensitivity had to be greatly enhanced. We have shown how this can be accomplished using localized states. These optimized charge detection techniques might be employed in the future to study the behavior of Coulomb dominated Fabry-Pérot interferometers in the FQH regime. Here, (time-resolved) charge detection techniques might allow to study quasiparticle charges and the inner structure of edge states, which are only accessible by direct transport in very special cases. Subsequently, we have investigated such a special case: here, the transport properties of a single QD were modified due to the presence of different compressible and incompressible regions in the dot. The transport behavior of the system could be described in analogy to the physics of a double quantum dot. Our results show that the inner structure of a QD can strongly influence the charging spectrum, which is relevant for Coulomb blockade experiments trying to investigate the statistics of the  $\nu=5/2$  edge excitations. Finally, transport in top-gate defined interferometers has been investigated. Here we have used different high-mobility 2DEGs that employ different doping techniques. We have investigated the experimental problems that arise, for example due to the lack of stability of the structures. We have demonstrated how a fully gapped  $\nu=5/2$  state can be confined in a top-gate defined interferometer without destroying the quantization, by careful choice of the 2DEG in combination with gating and illumination techniques. This is one of the experimentally most challenging prerequisites for the implementation of an interference experiment at  $\nu=5/2$  and has to our knowledge not yet been clearly demonstrated in literature. Unfortunately, no interference could be found at  $\nu=5/2$ . This was mainly attributed to an inappropriate QPC geometry. Implementing an optimized interferometer geometry with the techniques described by us, might in the future allow interference experiments at  $\nu=5/2$ .

The physics of the second LL is not only influenced by FQH states, but also by density modulated phases corresponding to the reentrant integer quantum Hall (RIQH) effect. A better understanding of the density-modulated phases might also improve our understanding of the physics of the second Landau level as a whole. Hence we have investigated the RIQH phases in non-equilibrium transport. Due to their extreme fragility and high requirements to the sample quality, only few research groups were able to investigate those states. Because of this, many properties of these phases are still unknown and are still under experimental study. Our results suggest that either these phases are not electron-hole symmetric as expected from theory or that they possibly are of a more complicated nature than anticipated. As these phases

reside in the same LL as the  $\nu=5/2$  state, such a particle-hole asymmetry might be of relevance for the physics at  $\nu=5/2$  and the groundstate that is formed at this filling factor.

## Organization of this book

This book is structured in five parts:

**Part I** gives an introduction to two-dimensional electron gases, the quantum Hall effect and edge states. We discuss the possibility of non-Abelian statistics and how this could be probed with interference experiments. Finally, we give a short overview of experiments at  $\nu=5/2$  by other authors and discuss their relevance for our results and whether they are compatible with our findings.

**Part II** describes how the measurement setup and samples were optimized, which in the end allowed us to perform experiments with the most fragile FQH states.

**Part III** discusses the QPC experiments: we start with investigating transport at zero magnetic field and the QPC confinement potential. Then we turn to the question of the magnetic field transmission of QPCs and how to observe a  $\nu=5/2$  state in a QPC. Finally, we discuss the quasiparticle tunneling experiments in the second LL.

**Part IV** shows the results of quantum dot and interferometer experiments. After a discussion of how charge detection techniques can be pushed towards the technical limit, we investigate a quantum dot, where the transport properties are strongly modified due to the presence of compressible and incompressible regions inside the dot. Then we discuss progress towards an interference experiment at  $\nu=5/2$ .

**Part V** summarizes the non-equilibrium transport measurements in the reentrant integer quantum Hall phases of the second Landau level.

## References

1. R.B. Laughlin, Phys. Rev. Lett. **50**, 1395 (1983). doi:[10.1103/PhysRevLett.50.1395](https://doi.org/10.1103/PhysRevLett.50.1395)
2. J.K. Jain, *Composite Fermions* (Cambridge University Press, Cambridge, 2007)
3. R. Willett, J.P. Eisenstein, H.L. Störmer, D.C. Tsui, A.C. Gossard, J.H. English, Phys. Rev. Lett. **59**, 1776 (1987). doi:[10.1103/PhysRevLett.59.1776](https://doi.org/10.1103/PhysRevLett.59.1776)
4. G. Moore, N. Read, Nucl. Phys. B **360**, 362 (1991). doi:[10.1016/0550-3213\(91\)90407-O](https://doi.org/10.1016/0550-3213(91)90407-O)
5. S.D. Sarma, M. Freedman, C. Nayak, Phys. Today **59**, 32 (2006). doi:[10.1063/1.2337825](https://doi.org/10.1063/1.2337825)

**Part I**

**Fundamentals of Quantum Hall Physics  
and Relevant Experiments**

# Chapter 2

## Two-Dimensional Electron Gases

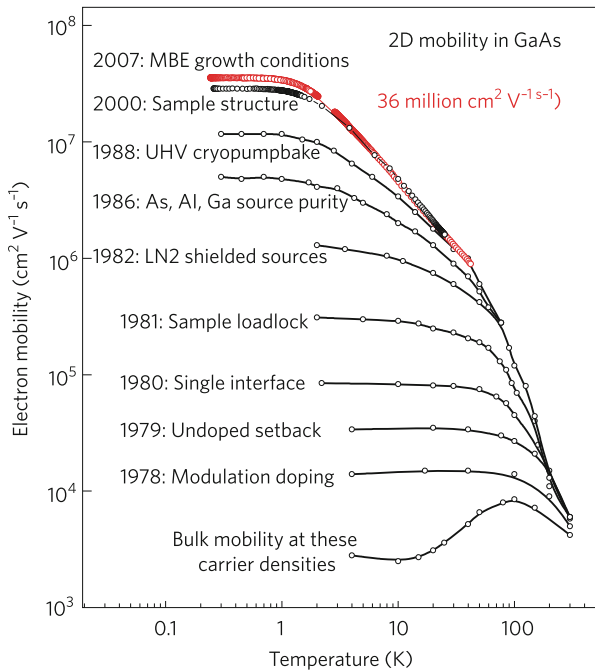
**Abstract** We review the basic low magnetic field properties of two-dimensional electron gases (2DEGs). The influence of growth techniques on the observation of the most fragile fractional quantum Hall states is discussed.

### 2.1 Introduction

Two-dimensional electron gases (2DEGs) in Gallium Arsenide (GaAs) represent the cleanest solid state system that is accessible to experimentalists. Continuous technological progress in molecular beam epitaxy (MBE) growth (Fig. 2.1), has allowed fabricating 2DEGs of higher and higher mobilities. In these systems new single- and many-body quantum phenomena, like the integer quantum Hall (IQH) effect and the fractional quantum Hall (FQH) effect, have been discovered. The Nobel prizes of 1985 (Klaus von Klitzing) and 1998 (Robert B. Laughlin, Horst L. Störmer and Daniel C. Tsui) attest the great importance of these discoveries and the large interest they have raised, not only in the solid state physics community.

More recent discoveries, like the exotic fractional quantum Hall (FQH) states at  $\nu = 5/2$  and  $\nu = 12/5$  show that still many interesting many-body phenomena remain to be studied in these systems. In the following, we will shortly review the basic properties and characteristics of 2DEGs. We will quickly discuss the sophisticated growth techniques that make the observation of exotic FQH states possible and hence provide the foundation for the experiments described in this book. Furthermore, these techniques have a large influence on the gating properties of top-gated structures, which is of great relevance for the experiments discussed later in this book.

**Fig. 2.1** Electron mobilities versus temperature for state-of-the-art GaAs 2DEGs grown in different years. The main lever for the mobility improvement is indicated for each curve. The best currently available 2DEGs reach mobilities of more than 30 million  $\text{cm}^2/\text{Vs}$  (Taken from [1]. Reprinted by permission from Macmillan Publishers Ltd)



## 2.2 Basic Properties of Two-Dimensional Electron Gases

The growth of two-dimensional AlGaAs/GaAs heterostructures relies on the combination of layers of GaAs with layers of the ternary compound  $\text{Al}_x\text{Ga}_{1-x}\text{As}$ . GaAs and AlAs have a small lattice mismatch of only 0.14 % [2], but different band gaps  $E_g$  ( $E_g = 1.424$  eV for GaAs and  $E_g = 2.168$  eV for AlAs [3]). Thus GaAs and  $\text{Al}_x\text{Ga}_{1-x}\text{As}$  layers can be combined without creating significant strain, but creating large discontinuities in the conduction band edge energy  $E_{\text{CB}}$ . Figure 2.2 illustrates how this technique is used to specifically engineer the conduction band edge, in order to create a two-dimensional electron gas. Figure 2.2a shows a layer sequence of a single-side doped heterostucture. A conduction band energy, obtained from numerically solving Poisson and Schrödinger equations self-consistently, is shown on the right hand side (Fig. 2.2b) as a function of the reversed growth direction  $z$ . The surface of the heterostructure is capped by a thin layer of GaAs to prevent oxidation. The conduction band bottom at the surface is raised due to surface reconstruction or due to a Schottky barrier with a metallic top-gate and is far above the Fermi energy  $E_F = 0$ . Below the GaAs cap, a thick layer of  $\text{Al}_{0.24}\text{Ga}_{0.76}\text{As}$  is grown, which leads to a discontinuity of the conduction band energy at the interface between these two materials. At  $z = 250$  nm, the conduction band energy is pinned close to the Fermi energy due to strong local doping with silicon (Si). At  $z > 320$  nm, another wide region of GaAs has been grown. Due to the pinning of the conduction band edge at

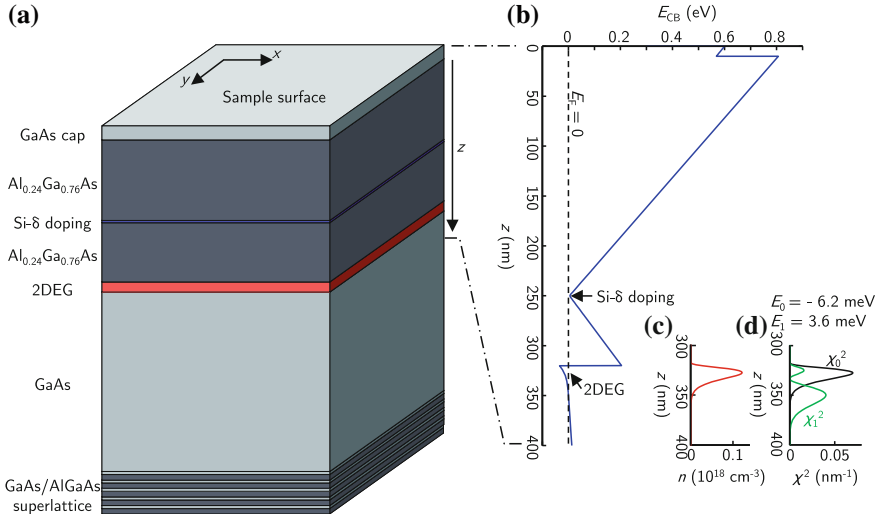


**Fig. 2.2** **a** Layer structure of a single-side doped high-mobility heterostructure. The conduction band edge, obtained from a numerical self-consistent solution of Poisson and Schrödinger equations is shown in **(b)**. The electron densities and *square* of the electronic wavefunctions of the two lowest subbands are shown in **c** and **d** as a function of  $z$ . Here, only the lowest subband has a negative eigenenergy and is occupied

the doping plane and due to the discontinuity of the conduction band at  $z = 320\text{ nm}$ , the conduction band edge is pulled below the Fermi energy at the interface between  $\text{Al}_x\text{Ga}_{1-x}\text{As}$  and GaAs. Here, free states in the conduction band are filled by electrons up to the Fermi energy, leading to a finite electron density close to the interface. The calculated electron density of the sample is shown in Fig. 2.2c. The conduction band electrons are confined in an approximately triangular confinement potential. The calculated square of the electron wavefunction in  $z$  direction,  $\chi^2(z)$ , is shown in Fig. 2.2d for the two lowest subbands ( $\chi_0^2$  and  $\chi_1^2$ ). In this situation, only the lowest subband, with an eigenenergy of  $E_0 = -6.2\text{ meV}$  is occupied, while the second subband with  $E_1 = 3.6\text{ meV}$  remains empty. In this situation, the electron wavefunction  $\psi(x, y, z)$  can be written as a plane wave for the in-plane directions  $x$  and  $y$  [4]:

$$\psi(x, y, z) = \chi(z)e^{i(k_x x + k_y y)} \quad (2.1)$$

with a parabolic dispersion relation [4]:

$$E_{n,\mathbf{k}} = E_n + \frac{\hbar^2}{2m^*}(k_x^2 + k_y^2) \quad (2.2)$$

We have used  $\mathbf{k} = (k_x, k_y)^T$ .  $E_n$  is the eigenenergy of the  $n$ th subband and  $m^*$  is the effective mass of the 2DEG electrons. In this situation, the small  $z$ -extent of the

volume occupied with electrons becomes negligible and we are dealing with a quasi two-dimensional system.

The following list comprises the most important quantities for the description of a 2DEG (partially taken from [4]). We give typical values of the quantities for a high mobility 2DEG with  $n_s \approx 2.5 \times 10^{11} \text{ cm}^{-2}$  and  $\mu \approx 20 \times 10^6 \text{ cm}^2/\text{Vs}$ .

**Electron density** The electron density mainly depends on the doping concentration and the thickness of the AlGaAs spacer between 2DEG and doping plane. Typical electron densities are of the order of  $1.0 \times 10^{11} \text{ cm}^{-2}$ – $1.7 \times 10^{11} \text{ cm}^{-2}$  for single-side doped heterostructures and  $2.0 \times 10^{11} \text{ cm}^{-2}$ – $3.5 \times 10^{11} \text{ cm}^{-2}$  for double-side doped quantum wells (QWs).

**Electron mobility** The electron mobility  $\mu$  relates to the effective mass  $m^*$  and the momentum relaxation time  $\tau$  via [4]:

$$\mu = \frac{e\tau}{m^*} \quad (2.3)$$

In the best samples available, typical magnitudes of the mobility are  $5 \times 10^6 \text{ cm}^2/\text{Vs}$ – $10 \times 10^6 \text{ cm}^2/\text{Vs}$  for single-side doped heterostructures and  $\mu \geq 15 \times 10^6 \text{ cm}^2/\text{Vs}$  for double-side doped QWs.

**Elastic mean free path** The elastic mean free path  $l_e$  is given as:

$$l_e = \tau v_F \quad (2.4)$$

where  $v_F$  is the Fermi velocity. In the best samples, the elastic mean free path can be as large as  $175 \mu\text{m}$ .

**Effective mass** The in-plane effective mass  $m_{\parallel}^*$  is given by [4]:

$$\frac{1}{m_{\parallel}^*} = \frac{p_A}{m_A^*} + \frac{p_B}{m_B^*} \quad (2.5)$$

Here,  $p_A$  and  $p_B$  are the probabilities for finding the electron in material A or B [4]. For typical 2DEGs, the envelope of the electronic wavefunction is small outside the GaAs region in which the 2DEG is defined. Hence, the in-plane effective mass corresponds with a good accuracy to the bulk GaAs effective mass:  $m_{\parallel}^* \approx m_{\text{GaAs}}^* \approx 0.063 m_e$  [3].

**Density of states** The parabolic dispersion relation leads to a constant density of states:

$$\mathcal{D}_{2d}(E) = \frac{g_s m^*}{2\pi\hbar^2} \quad (2.6)$$

where  $g_s$  denotes the spin degeneracy.

**Fermi energy** The Fermi energy of the two-dimensional system is given as:

$$E_F = \frac{2\pi n_s \hbar^2}{g_s m^*} \quad (2.7)$$

In typical high-mobility 2DEGs,  $E_F \approx 30$  meV is found.

**Fermi wavevector** The Fermi wavevector is defined as:

$$k_F = \sqrt{\frac{4\pi n_s}{g_s}} \quad (2.8)$$

It has a typical size of  $k_F \approx 1.3 \times 10^8$  m<sup>-1</sup>.

**Fermi wavelength** From this, the Fermi wavelength is obtained:

$$\lambda_F = \sqrt{\frac{g_s \pi}{n_s}} \quad (2.9)$$

where typically  $\lambda_F \approx 50$  nm in our samples.

**Fermi velocity** The Fermi velocity is the group velocity of an electron at the Fermi energy and is given by:

$$v_F = \frac{\hbar k_F}{m^*} \quad (2.10)$$

For our samples we find  $v_F \approx 2.4 \times 10^5$  m/s.

**Classical cyclotron radius** The cyclotron radius is the radius of a classical circular orbit described by an electron in a magnetic field  $B$  due to the Lorentz force:

$$R_c = \frac{\hbar k_F}{e B} \quad (2.11)$$

At a given magnetic field  $B$ , we find:  $R_c \times B \approx 85$  nmT.

**Magnetic length** The magnetic length at a given magnetic field  $B$  is given as:

$$l_B = \sqrt{\hbar/eB} \quad (2.12)$$

Typical magnetic lengths in quantum Hall experiments are of the order of 10 nm:  $l_B \times \sqrt{B} = 25.6$  nm $\sqrt{\text{T}}$ .

**Cyclotron energy** Using the cyclotron frequency  $\omega_c = \frac{eB}{m^*}$ , the cyclotron energy  $E_{cyc}$  is given as:

$$E_{cyc} = \hbar \omega_c = \frac{\hbar e B}{m^*} \quad (2.13)$$

Expressed in terms of thermal energy  $k_B T$ , the cyclotron energy corresponds to:  $\frac{E_{cyc}}{B} \hat{=} 20$  K.

**Coulomb energy** The Coulomb energy is given as [5]:

$$E_{Coulomb} = \frac{e^2}{4\pi\varepsilon\varepsilon_0 l_B} \quad (2.14)$$

Here,  $\varepsilon_0$  denotes the vacuum permittivity and  $\varepsilon$  the relative dielectric constant (in our case GaAs:  $\varepsilon = 12.9$ ). Expressed in terms of thermal energy, this corresponds to:  $\frac{E_{Coulomb}}{\sqrt{B}} \hat{=} 50.8$  K.

**Zeeman energy** The size of the Zeeman splitting is given as [6]:

$$E_Z = 2g\mu_B \mathbf{B} \cdot \mathbf{S} = \frac{g m^*}{2 m_e} \hbar \omega_c \quad (2.15)$$

where  $m_e$  is the mass of a free electron. In bulk GaAs, the size of the Zeeman splitting corresponds to:  $\frac{E_Z}{B} \hat{=} 0.3$  K. In reality, the effective  $g$ -factor and also the Zeeman splitting can be strongly enhanced.

## 2.3 Low Field Magnetoresistance of Two-Dimensional Electron Gases

A classical Hall measurement [7] at low magnetic fields can be performed in a setup depicted in Fig. 2.3. Here, a four-terminal measurement scheme is used, where the current is passed in the  $x$ -direction along the long axis of the Hall-bar. A homogeneous external magnetic field  $B$  is applied perpendicular to the 2DEG. The voltages  $V_{xx}$

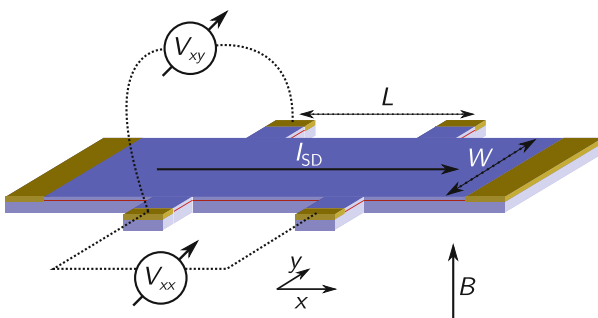


**Fig. 2.3** Hall-bar measurement configuration. While a current  $I_{SD}$  is passed along the long axis of the Hall-bar, voltages  $V_{xx}$  and  $V_{xy}$  are measured. The voltage contacts define an area of a geometry factor  $(W/L)$ . An external magnetic field  $B$  is applied perpendicular the 2DEG plane

and  $V_{xy}$  are measured on separate voltage contacts that define a geometry factor  $(W/L)$ .

In two dimensions, the electric field  $\mathbf{E} = (E_x, E_y)^T$  and the current density  $\mathbf{j} = (j_x, j_y)^T$  are related via:

$$\begin{pmatrix} E_x \\ E_y \end{pmatrix} = \begin{pmatrix} \rho_{xx} & \rho_{xy} \\ \rho_{yx} & \rho_{yy} \end{pmatrix} \begin{pmatrix} j_x \\ j_y \end{pmatrix} \quad (2.16)$$

In the configuration of Fig. 2.3, we have  $j_x = I_{SD}/W$  and  $j_y = 0$ . Hence we can relate the components of the resistivity tensor to our measurement quantities via  $\rho_{xx} = (W/L) \frac{V_{xx}}{I_{SD}}$  and  $\rho_{xy} = \frac{V_{xy}}{I_{SD}}$ .

**Classical diffusive transport** At low magnetic fields when quantization effects are absent, the transport properties of the system can be well described by the Drude model [8]. With an external electric field  $\mathbf{E}$  and a magnetic field  $\mathbf{B}$ , the equation of motion of an electron between two scattering events can be written as [4]:

$$m^* \frac{d\mathbf{v}}{dt} = -|e|(\mathbf{E} + \mathbf{v} \times \mathbf{B}) \quad (2.17)$$

Scattering processes can be taken into account by assuming a statistical distribution of scattering angles and scattering times. Taking this statistical averaging into account, the components of the drift velocity  $\mathbf{v}_D = (\bar{v}_x, \bar{v}_y)^T$  can be found [4]. At  $B = 0$ , the following relation between the external electric field  $\mathbf{E}$  and the drift velocity  $\bar{v}_x$  is found:

$$\bar{v}_x = - \underbrace{\frac{e\tau}{m^*}}_{\mu} E_x = -\mu E_x \quad (2.18)$$

Here  $\mu$  is the electron mobility. Using the definition of the current density,  $\mathbf{j} = -n_s |e| \mathbf{v}_D$  and (2.16) we find [4]:

$$\rho_{xx} = \frac{m^*}{n_s e^2 \tau} \quad (2.19)$$

$$\rho_{xy} = \frac{B}{|e| n_s} \quad (2.20)$$

These measurement quantities are connected to the electron density and mobility via:

$$n_s = \frac{1}{|e| d\rho_{xy}/dB|_{B=0}} \quad (2.21)$$

$$\mu = \frac{d\rho_{xy}/dB|_{B=0}}{\rho_{xx}(B=0)} \quad (2.22)$$

## 2.4 Growth Schemes for High Electron Mobilities

High mobility quantum wells used for the experiments presented in this book were grown in the group of Werner Wegscheider at ETH Zürich, by Christian Reichl and Werner Wegscheider. The MBE system in use is optimized for highly pure MBE growth and incorporates only a very small amount of residual background impurities in the wafers. The technical challenges that arise for the growth of a high-mobility 2DEG, for example providing pure metal sources and optimized growth temperature, -rate, etc. are far beyond the scope of this book. A discussion with respect to an optimization of 2DEGs for the observation of the  $\nu = 5/2$  state can for example be found in [9].

However, the doping schemes employed for the 2DEGs are of great experimental relevance. Thus we will give a short overview of the different techniques used. The details of the doping strongly influence the gating properties of a heterostructure and hence influence the behavior of top-gate defined devices. The samples that have been used for the experiments presented in this book employ either conventional DX-doping or quantum-well doping and are optimized for the formation of a pronounced  $\nu = 5/2$  state without the requirement of prior illumination with a light emitting diode (LED) [9]. For DX-doping, a  $\delta$ -doping plane of Si dopants is located in a wide  $\text{Al}_x\text{Ga}_{1-x}\text{As}$  region. Apart from the shallow donors with hydrogenic energy levels, deep donor levels, the DX-centers exist. Here, the binding of an electron involves a lattice deformation and leads to a strongly bound electron state [10, 11]. The energy difference between conduction band edge and DX energy level,  $\Delta_{\text{DX}}$ , scales linearly for  $0.22 < x < 0.4$  (from  $\Delta_{\text{DX}} = 0$  at  $x = 0.22$  to  $\Delta_{\text{DX}} = -0.16$  eV at  $x = 0.4$ ) [12]. Hence DX centers become shallow energy levels for a small Al mole fraction. Illuminating a DX-doped sample at low temperatures ionizes the electrons bound in DX-centers and enhances the electron density. We will discuss in the next section why illumination is often necessary in such samples, in order to observe a quantized  $\nu = 5/2$  state.

An example of a DX-doped structure is shown in Fig. 2.4a. The corresponding schematics of the conduction band edge is shown in Fig. 2.4b. Here a 27 nm wide QW is defined approximately 200 nm below the surface and a DX-doping scheme in  $\text{Al}_{0.24}\text{Ga}_{0.76}\text{As}$  is used, at a setback distance of approximately 100 nm. Within the  $\text{Al}_{0.24}\text{Ga}_{0.76}\text{As}$  spacers, two 1.5 nm wide GaAs QWs are defined, which are expected to provide additional screening of the QW from long-range remote impurity scattering. However, without illumination of the sample, these narrow QWs are not expected to be occupied by charge carriers.<sup>1</sup>

Quantum well doping [13–15] is an efficient technique for screening the 2DEG from long-range remote impurity scattering. Here, the doping region consists of a narrow GaAs quantum well, defined between thin barriers of AlAs [9]. The  $\delta$ -Si doping plane lies in the center of the narrow GaAs QW, hence no DX centers are formed [10]. When the layer thicknesses are chosen appropriately, the X-band minima of the AlAs layers reside below the conduction band edge of the narrow GaAs

---

<sup>1</sup>C. Reichl, private communication.

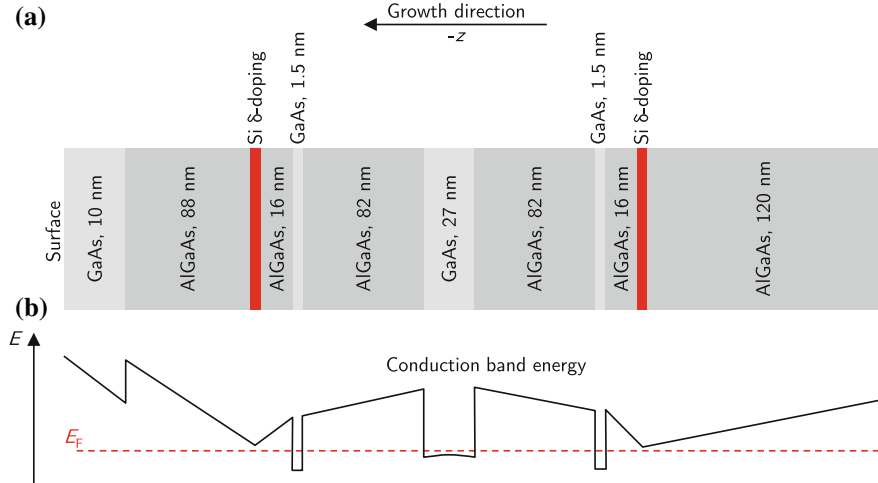


**Fig. 2.4** **a** Layer sequence of a 27 nm wide QW grown 200 nm below the sample surface and using a DX-doping scheme. **b** Schematic conduction band energy as a function of position. The *dashed red line* indicates the Fermi energy

quantum wells ( $\Gamma$ -band) and excess electrons occupy the AlAs X-band [15]. The high effective mass X-band electrons provide additional screening of the 2DEG from long range potential fluctuations [9], but do not contribute to the 2DEG conductance if the growth parameters are suitably chosen.

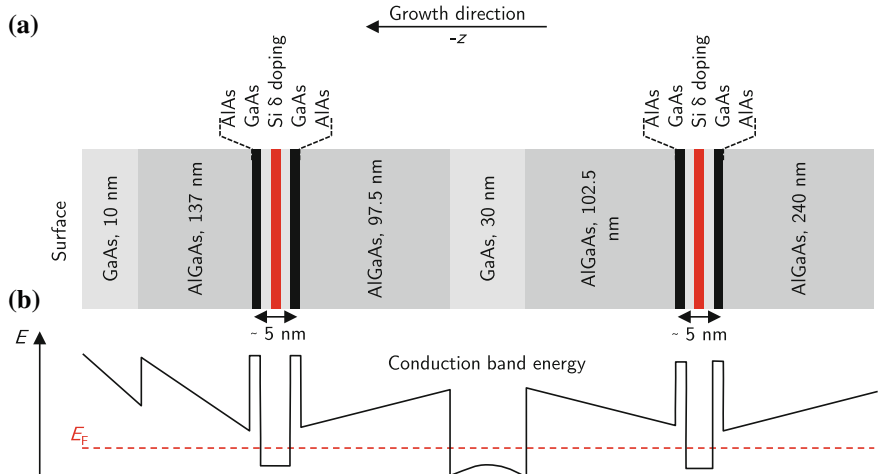


**Fig. 2.5** **a** Layer sequence of a 30 nm wide QW grown 250 nm below the sample surface and using a QW-doping scheme. **b** Schematic conduction band energy as a function of position. The *dashed red line* indicates the Fermi energy